Journal of Materials Chemistry C

Accepted Manuscript

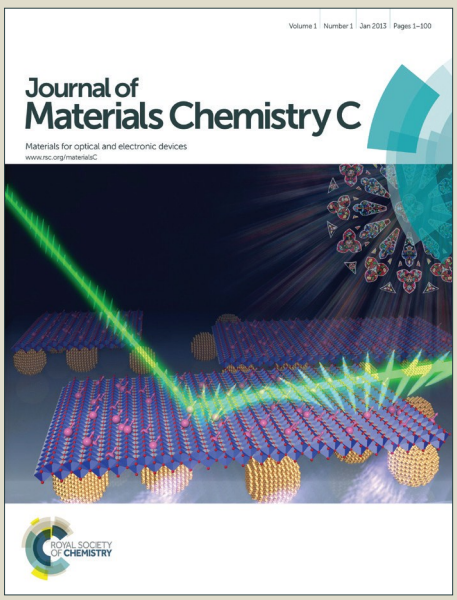

ROYAL SOCIETY OF CHEMISTRY

www.rsc.org/materialsC

Exploring Local Electronic Structure and Geometric Arrangement of ALD Zn(O,S) Buffer Layers using X-Ray Absorption Spectroscopy

Anup Dadlani[‡,1] *Orlando Trejo*[‡,2] *Shinjita Acharya*[‡,2] *Jan Torgersen,*[2] *Ioannis Petousis,*[3] *Dennis Nordlund,*[4] *Ritimukta Sarangi,*[4] *Peter Schindler,*[2] *and Fritz B. Prinz**[2,3]

[1] Department of Chemistry, Stanford University, Stanford, CA 94305

[2] Department of Mechanical Engineering, Stanford University, Stanford, CA 94305, USA

[3] Department of Materials Science and Engineering, Stanford University, Stanford, CA 94305, USA

[4] Stanford Synchrotron Radiation Lightsource, SLAC National Accelerator Laboratory, Menlo Park, CA 94025, USA

‡ These authors contributed equally to this work

* To whom correspondence should be addressed - fprinz@stanford.edu

Abstract: The growing interest in zinc oxysulfide (Zn(O,S)) thin films as buffer layers has been motivated by higher efficiencies achieved in solar cells. In this work we present insights toward the electronic-geometric structure relationship of varying compositions of Zn(O,S) grown by atomic layer deposition (ALD). X-ray absorption near edge structure (XANES), a local bonding-sensitive spectroscopic tool, with quantum simulations help link atomic structure to the unoccupied density of states (DOS) of the films. The infiltration of sulfur into a ZnO matrix results in the formation of S 3p – Zn 4sp – O 2p hybridized orbitals in the near edge X-ray absorption fine structure (NEXAFS) region of both the O and S K-edges. The extent of sulfur incorporation affects the ionicity of Zn; which in turn alters the bond lengths of Zn – O within the structure and its resulting bandgap. Knowing zinc oxyfulfide's electronic-geometric structure interplay allows one to predict, tailor, and optimize its buffer layer performance.

KEYWORDS X-ray absorption near edge structure (XANES), local density of states (LDOS), Zn(O,S), atomic layer deposition (ALD), oxysulfide films

Introduction

Zinc oxysulfide (Zn(O,S)) thin films have been successfully used as phosphor host materials[1] and photocatalysts,[2] but have lately seen a rapid rise in its utility as a buffer layer in solar cells due to its compositional and crystal structure tunability. Varying its composition, key parameters like bandgap, conduction band offset, and conductivity can be precisely tuned.[3, 4, 5, 6, 7] In addition to the need for great functional tunability, buffer layers should also be non-toxic[8] and earth abundant[9] in order to be environmentally safe and applicable in low cost production.[10] Owing to its versatility, Zn(O,S) fits all these criteria and is therefore a promising candidate to replace the conventional CdS as a buffer layer since it is compatible with various absorber layers (SnS, CIGS, CIS, CZTS) and has a large bandgap (E_g~2.6-3.8eV).[11] A large bandgap reduces photocurrent loss in the short wavelength region, allowing a greater collection of high-energy electrons. Also careful adjustment of the sulfur content leads to minimization of recombination at the buffer interface.[12] Though device specific electronic properties have been related to different Zn(O,S) compositions using X-ray photoelectron spectroscopy (XPS) and UV-vis,[4,7,12] deeper insight into the electronic structure of the films is required to understand the nature of chemical composition effects. X-ray absorption near edge structure (XANES) technique is a suitable probe, capable of revealing oxidation states, coordination chemistry, molecular orbitals, band structure, local displacement and chemical short-range order information.[13]

To gain insight into the electronic-geometric structure relationship of Zn(O,S) films depending on their O/S content, XANES was performed. In an iterative process, structural solutions were established by simulating various atomic arrangements using density functional theory (DFT). These structures were used as inputs for ab-initio calculations of the respective XANES spectra using FEFF code. The structural changes associated with incorporation of sulfur led to an increase in the ionicity of Zn, manifested by an increase in the bond length of Zn – O. On the other hand, it also lead to a decrease in bandgap; both of which have profound effects on the performance of Zn(O,S) as a buffer layer. Lastly, ligand field theory provided a greater understanding into the local bonding environment at the lowest lying states of the conduction band.

Allowing atomic scale control of film thickness and composition, atomic layer deposition (ALD) enables the necessary fine-tuning of the Zn(O,S) system.[10,14,15,16,17] ALD was used to deposit Zn(O,S) by alternating sequences of diethylzinc (DEZ), H_2O and H_2S exposures, where zinc oxysulfide formation was suggested to proceed via the incorporation of sulfur in the ZnO matrix, causing changes to the local bonding environment.[7,18,19]

The samples investigated were labeled as follows – ZnO and ZnS ALD films, which served as our references. The Zn(O,S) films were labeled as 10, 20, and 33%, corresponding to H_2S pulses to total oxidant pulses in the deposition. All films (300 cycles) were deposited on nanostructured anatase TiO_2 nanoparticles (NPs) (details in ESI). The prepared ALD Zn(O,S) films were characterized by XPS, atomic force microscopy (AFM), X-ray reflectivity (XRR), UV-vis, and X-ray diffraction (XRD) measurements, where satisfactory agreement was obtained to what has been observed in literature (refer to ESI for additional details).

To elaborate on the local bonding environment of oxygen, a comparison of XANES spectra at the O K-edge in Zn(O,S) along with simulated spectra for each sample, has been presented in Fig. 1a. Through an iterative process, DFT-derived structures were simulated in FEFF by changing self-consistent field (SCF) and full multiple scattering (FMS) parameters (details in ESI). Of the simulations that were performed, clusters containing 0%, 6.25%, 12.5%, and 25% sulfur incorporated into a ZnO wurtzite structure were found to be the closest match to the experimental ZnO, 10%, 20%, and 33% samples respectively (see ESI for more details). Multiple scattering (MS) calculations were also performed (Fig. 1b) on different cluster sizes to distinguish the features mainly arising from multiple scattering effects.

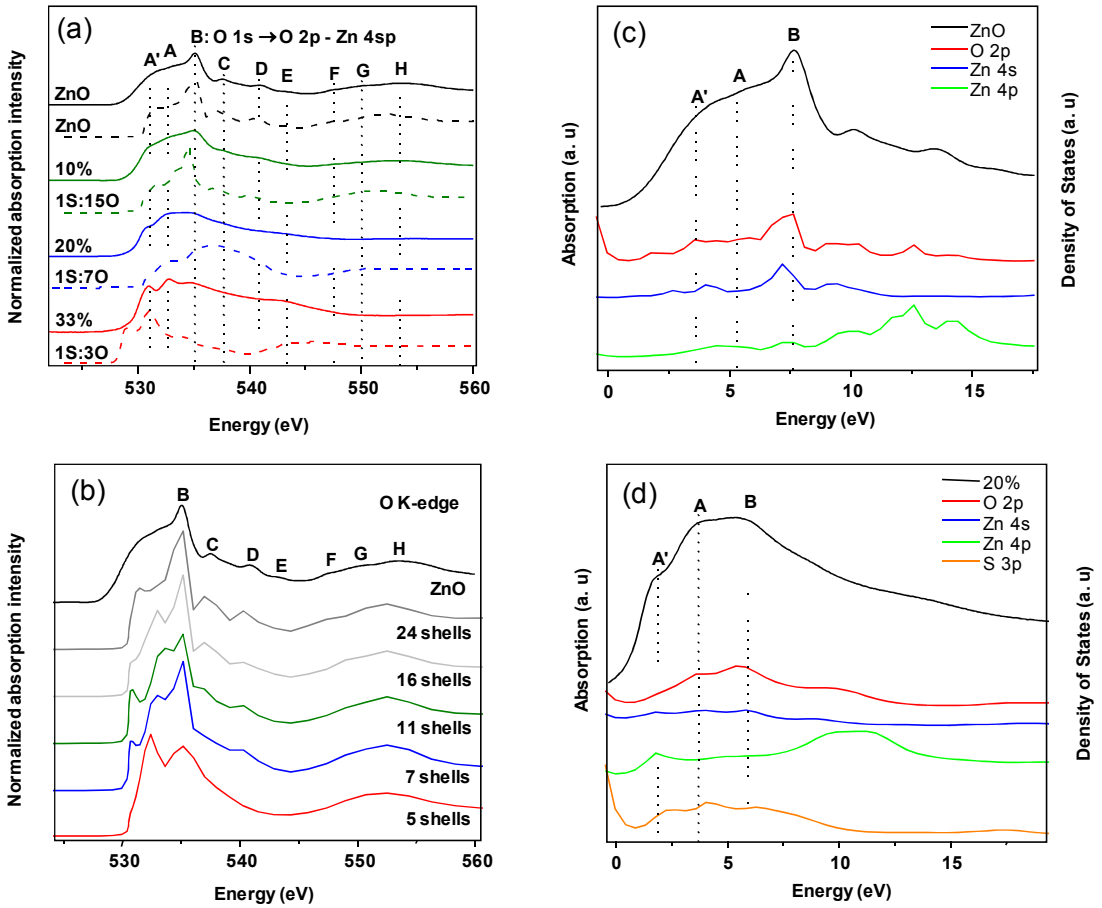

Fig. 1. X-ray absorption characterization at O K edge are shown for Zn(O,S) films deposited on anatase TiO_2. All experimental curves (solid) are accompanied by simulated curves (dotted) shown underneath, obtained using FEFF code.[20, 21] ZnO reference, 10%, 20%, and 33% samples, where the best matching simulations were determined to be structures containing 0%, 6.25%, 12.5%, and 25% sulfur respectively at (a) O K-edge spectra were background subtracted and atomically normalized in the energy region from 548 to 560 eV. (b) Theoretical MS calculations done in FEFF for the O K-edge as a function of the cluster size for wurtzite ZnO for clusters with increasing atomic shells: 5, 7, 11, 16 and 24. A shell refers to a group of atoms at a particular distance from the absorbing atom. The 24-shell cluster corresponds to a sphere of radius 10 Å. The experimental ZnO curve is shown above as a reference. Feature D first develops after 7 shells (mid-range order) are considered, while feature C appears with 11 shells (long-range order); both features are pre-dominantly a result of multiple scattering. Spacing between features C and D is 3.3 eV, same as in the

experimental curves. (c) Calculations of the partial density of states (pDOS) relative to the Fermi level (total density of states shifted so onset of bandgap is at 0 eV) plotted together with the experimental XAS spectra (XAS spectrum aligned by matching max intensity to max pDOS intensity of absorbing atom) for ZnO, showing that O 2p, Zn 4s, and Zn 4p contribute to the conduction band. (d) 20% oxysulfide shows contributions from S 3p orbitals to the already present O 2p and Zn 4sp orbitals (especially near the main edge). pDOS for other stoichiometries are provided in ESI.

Fig. 1a, has eight main features that appear in the total electron yield O K-edge XANES, labeled A – H for the ZnO reference sample, similar to what is observed in literature.[22] The features A - G have been broadly assigned to the electronic excitation from O 1s states to unoccupied states in the conduction band of ZnO, which is made up of O 2p – Zn 4sp states (Fig. 1c).[22] The simulated curve closely matches the experimental curve, only missing peak E. As from Fig. 1b, peaks C (long-range order) and D (mid-range order) mainly arise from multiple scattering and are slightly shifted. The 10% sample bears great resemblance to reference ZnO which was expected given it contains the least S causing almost no change in the O environment in the ZnO. The intensity ratio of B/A has decreased. The increase in A along with the apparent broadening indicates a distortion in the local bonding environment with the incorporation of sulfur, which also affected the orbital mixing. The simulation curve hinted that these slight distortions from wurtzite ZnO (confirmed by XRD, Fig. S4) impacted peaks C and D most, causing a decrease in intensity as expected.

The 20% sample was missing features C, D, and feature E was weaker and broader than the reference. Feature A was further increased (relative to B) partly due to sulfur's orbital contribution at the lower energies (Fig. 4b). There is also the rise of a pre-edge shoulder, peak A'. In general, the spectral weight is shifted to lower energies, nearer to the bottom of the conduction band with increasing S concentration. The bonding environment was more distorted than 10%, corroborated by both XANES and XRD (Fig. S4). The simulation using 12.5% sulfur shows the development of feature A' and has similar intensities for peaks A and B like the experimental curve. We did not expect the simulation to depict the fine structure at higher energies since we could not simulate all possible local environments that

are present within the sample. However, it captures the salient features present in the near edge region.

The 33% sample exhibits the greatest change amongst all the spectra, being both the broadest and most weight shifted to the lower energies. Peaks C and D are not visible, although there is a prominent peak at E, which is mainly attributed to multiple scattering because of a low density of states (DOS) there (Fig. S6). Features A and B are again resolved, but the greatest intensity has shifted to peak A. The main difference is that peak A' is now entirely resolved, no longer appearing as a shoulder. Clearly the nature of the hybridized states in the conduction band has been modified to produce more distinct resonances in the near edge with O 2p character changing both the structure and the spectrum that is observed.

Since we cannot directly observe O 1s → S 3p, this indicates that the S 3p is hybridized with the O 2p – Zn 4sp band, and we are observing transitions to O 2p – Zn 4sp – S 3p states. The partial DOS (pDOS) calculations supported this claim. In Fig. 1c, the pDOS of the simulated wurtzite ZnO as calculated in FEFF along with the experimental ZnO spectrum (alignment is further explained in ESI) has been shown. We clearly observe the participation of O 2p, Zn 4s, and Zn 4p orbital contributions in the conduction band of ZnO.[22] In the case of the oxysulfide compound (20% Zn(O,S) in Fig. 1d), the pDOS shows contributions coming from O 2p, Zn 4s, Zn 4p and S 3p orbitals. The S 3p contribution is particularly strong near the onset of the XANES spectrum, thus validating our claim.

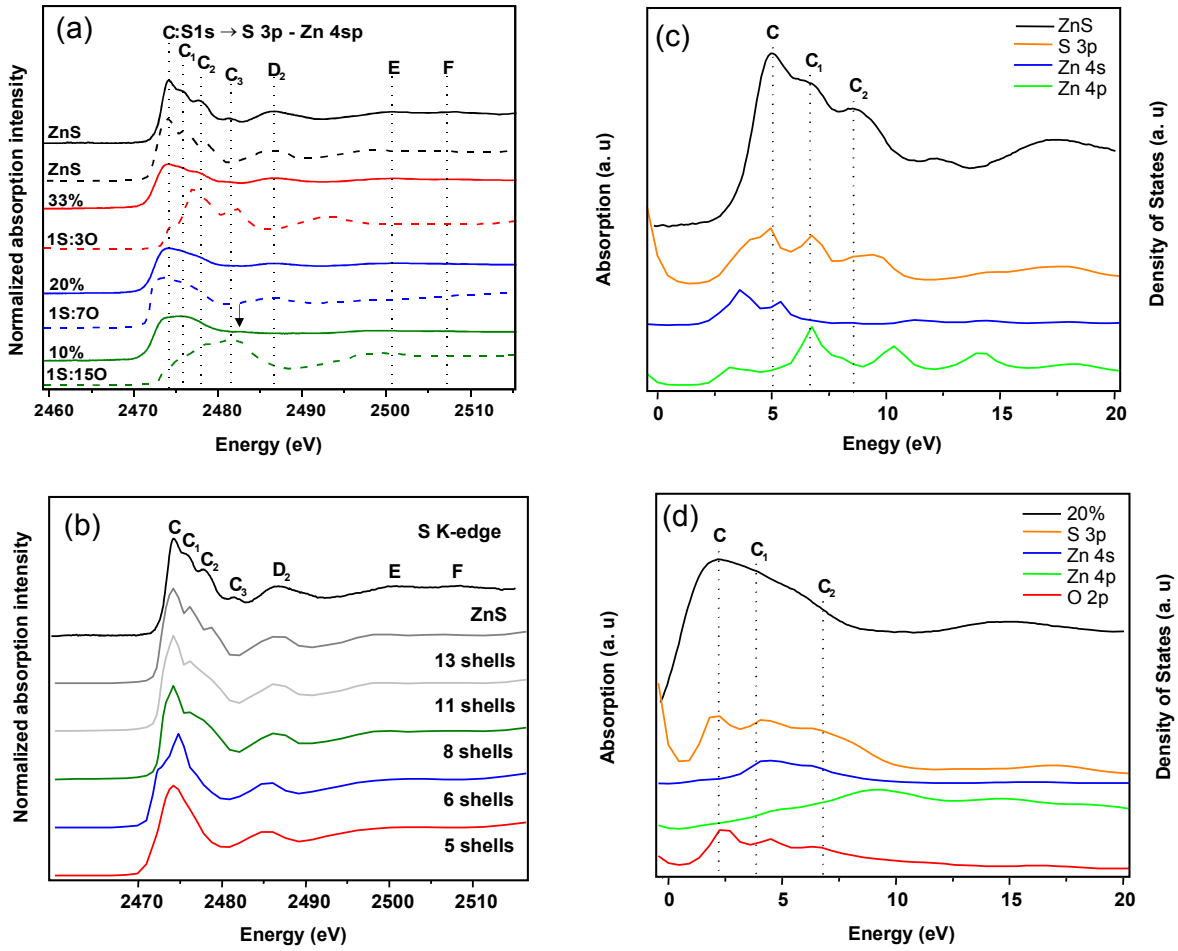

Fig. 2. X-ray absorption characterization at S K-edge is shown for Zn(O,S) films deposited on anatase TiO_2. All experimental curves (solid) are accompanied by simulated curves (dotted) shown underneath, obtained using FEFF code.[20, 21] ZnS reference, 10%, 20%, and 33% samples, where the best matched simulations were structures containing 0%, 6.25%, 12.5%, and 25% sulfur respectively at (a) S K-edge spectra were background subtracted and atomically normalized in the energy region from 2500 to 2510 eV. (b) Theoretical MS calculations at the S K-edge as a function of the cluster size for ZnS for clusters with increasing atomic shells: 5, 6, 8, 11 and 13. The 13-shell cluster corresponds to a sphere of radius 10 Å. The experimental ZnS curve is shown above as a reference. Feature C_1 develops when 8 shells (mid-range order) are considered and C_2 appears when 13 shells (long-range order) are considered, pertaining to multiple scattering. Calculations of the partial density of states (pDOS) relative to the Fermi level (total density of states shifted so onset of bandgap is at 0 eV) plotted together with the experimental XAS spectra (XAS

spectrum aligned by matching max intensity to max pDOS intensity of absorbing atom) for (c) ZnS which shows contribution from S 3p and Zn 4sp. (d) 20% at S edge showing contributions from S 3p, Zn 4sp, and O 2p. pDOS for other stoichiometries are provided in ESI.

Next, we investigated the S K-edge XANES spectra for all these samples. As a reference sample, ALD ZnS 300 cycles was grown on TiO_2 NPs. Seven main features appear in the total fluorescence yield S K-edge XANES spectrum (Fig. 2a), labeled C – C_3, D_2, E, and F for the reference sample matching previous observations.[23, 24, 25, 26, 27, 28] Feature C corresponds to an electronic excitation from S 1s state to unoccupied states in the conduction band of ZnS, which is composed primarily of S 3p and Zn 4sp orbitals (refer to Fig. 2c). Feature D_2 comprises of a combination of S 1s transition to an empty S p orbital along with multiple scattering effects (Fig. 2c).[24, 27, 28] The FEFF MS simulations indicates that features C_1 and C_2 predominantly appear as a result of mid-range and long-range order respectively for sphalerite ZnS shown in Fig. 2b. Overall there is agreement between the experiment and simulation, only feature C_3 is not captured by simulation.

The 33% sample has all the peaks as the reference sample, but every single feature after the main edge is less pronounced. The transition is no longer simply from S 1s transition to S 3p - Zn 4sp[29] hybridized orbitals as for ZnS. As observed for the O K-edge XAS and the pDOS calculations for this composition (Figures 1a and Fig. S6), there is mixing with O 2p leading to hybridized S 3p – Zn 4sp – O 2p states near the onset of the conduction band. The simulation retains the general shape at the lower energies.

The 20% sample maintains the overall shape of the reference ZnS film but entirely loses C_3. This loss of C_3 certainly suggests the long—range order or local atomic arrangement is not wurtzite or spahlerite ZnS.[23] The simulated curve matches almost exactly, showing a dulling of features C_1 and C_2, corresponding to a loss in mid and long-range order (Fig. 2b).

Finally, 10% is nearly featureless compared to all other stoichiometries. This lack of features might be a result of self-absorption. However, this can be ruled out because it has the least amount of sulfur and it would be likely that the other samples too would exhibit this effect. Instead it seems that features are missing because the sulfur present in the film is actually in many different environments. In other words, there is a compositional

heterogeneity of sulfur within the sample. In the case of 10%, the changes are attributed to a significantly distorted structure from cubic ZnS. One feature that begins to appear in this particular stoichiometry is located at 2482.6 eV (marked by the arrow) which indicates the presence of sulfate[30] (sulfur in +6 state). The simulated curve captures the severe broadening and loss of features as seen in 10%. Other than the small sulfate peak, we note that a lack of overall energy shifts for all spectra indicates that the sulfur oxidation state remains -2 for all samples.

A summary of the XANES peak identification for both the O-K and S-K edges have been provided below in Table 1.

Table 1. *O and S K-edge features and qualitative assignments for Zn(O,S). MS = multiple scattering and its assignment means it is a major contributor to that particular peak. Assignment of hybridized states means that it is a contributor of a peak along with short- and long-range orders.*

O K-edge			**S K-edge**		
Label	Energy (eV)	Assignment	Label	Energy (eV)	Assignment
A’	531.1	O 1s → O 2p – Zn 4sp – S 3p	C	2474.2	S 1s → S 3p – Zn 4sp – O 2p
A	532.9	O 1s → O 2p – Zn 4sp – S 3p	C_1	2476.2	MS (8 shells mid-range order)
B	535	O 1s → O 2p – Zn 4sp – S 3p	C_2	2478	MS (13 shells mid-range order)
C	537.5	MS (11 shells mid-range order)	C_3	2481.4	MS (long-range order)
D	541	MS (7 shells mid-range order)	D_2	2486.8	S 1s → S 3p – Zn 4p + MS
E	543.3	MS (long-range order)			

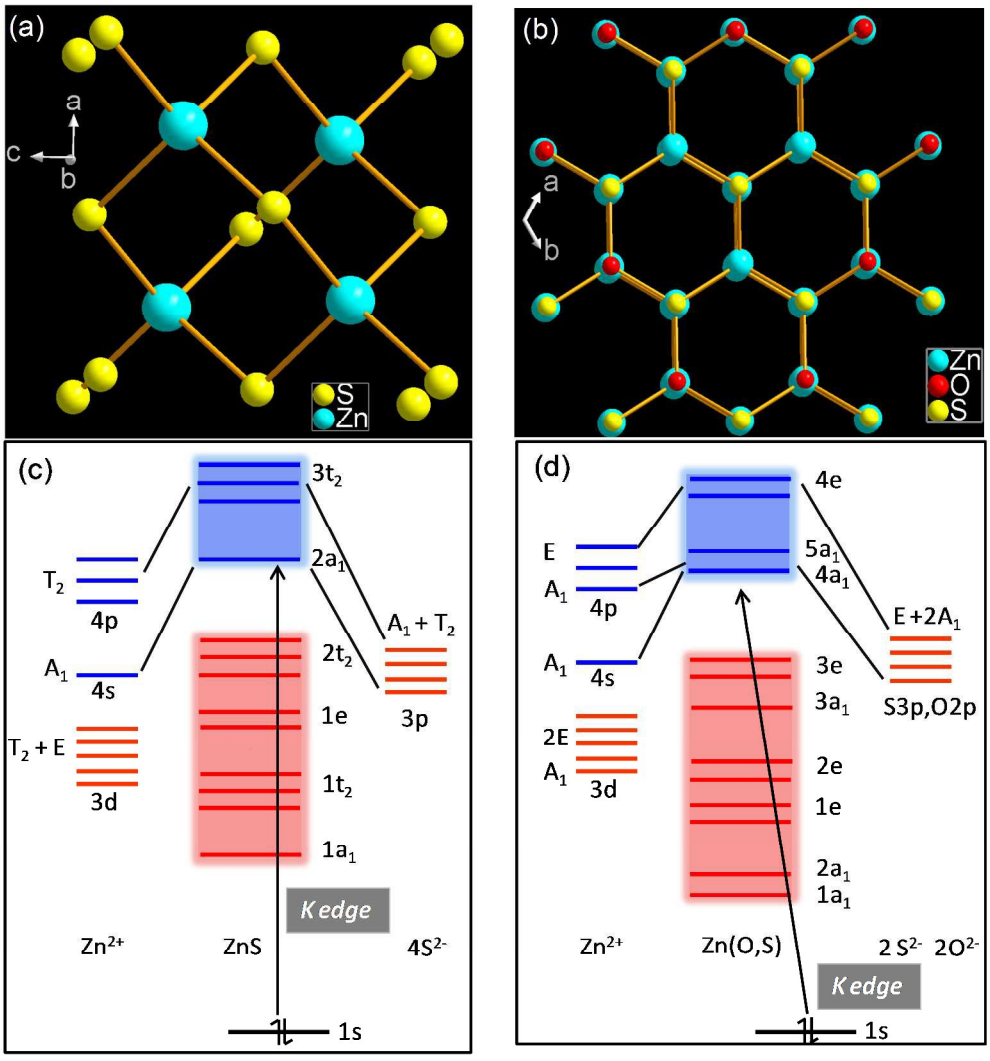

Fig. 3. Crystallographic models of ZnS crystal which was approximated to (a) T_d symmetry point group and (b) C_{3v} symmetry point group for a ZnO crystal with 50% sulfur (O/S = 1) incorporated. (c) The MO band energy diagram for ZnS implies that the conduction band (blue) is made up of antibonding orbitals contributed from both Zn 4sp and S 3p. (d) The MO diagram for Zn(O,S) (O/S=1) which shows that the conduction band (blue) is made up of Zn 4sp, O 2p and S 3p hybridized antibonding orbitals. The energy levels and energy gaps in the MO diagram are not drawn to scale. The lines from the atomic orbitals have only been drawn to the conduction band to simplify the schematic. Red orbitals means filled with electrons. Blue means empty orbitals. We are probing the transition of an electron from S 1s to the conduction band of the film by doing S K-edge XANES.

To gain a deeper understanding into the pDOS of oxysulfide Zn(O,S) films, we used ligand field theory to provide a qualitative picture of the orbital mixing for two particular cases. T_d symmetry was assumed for cubic ZnS (Fig. 3a); in the case of a 50-50 mix of S and O atomic percentages (representative of the 20% sample according to XPS) the point group becomes C_{3v} (Fig. 3b). Using the character tables from group theory we constructed the respective molecular orbital (MO) diagrams and ascertained the participation of the atomic orbitals to the occupied and unoccupied states (Fig. 3c, d). From this simplistic view we were able to extract the nature of the bonding along with the contribution of individual orbitals to particular states. Here we can attribute the lowest allowed transitions into the conduction band for both ZnS and Zn(O,S) as having a_1 symmetry. In the case of ZnS, the lowest lying state is made up of S 3p - Zn 4s hybridized orbitals, while the higher available states are composed of S 3p – Zn 4p hybridized orbitals, which is supported by pDOS (Fig. 2c). For Zn(O,S), the lowest accessible state is composed of O 2p – S 3p – Zn $4sp_z$ hybridized orbitals, also corroborated by pDOS (Fig. 2d). In both cases we see that the excitation of an 1s electron from sulfur into Zn 4s, which is typically not allowed by dipole selection rules, takes place due to orbital mixing with anion p orbitals having the appropriate symmetry.

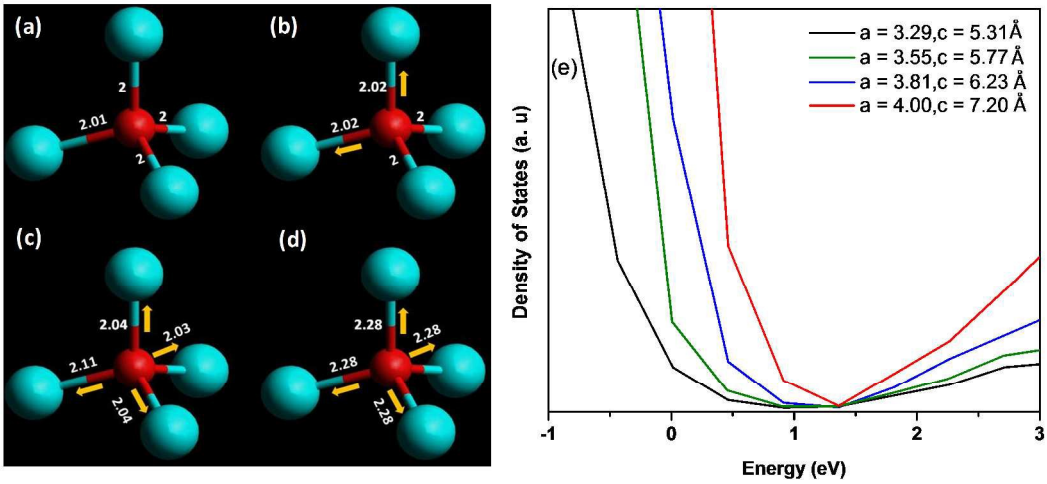

Fig. 4. (a) Bond distances of ZnO tetrahedrons in different stoichiometric structures obtained from VASP (also used for FEFF simulations) are shown for (a) ZnO (b) 1S:15O structure best matched 10% sample (c) 1S:7O structure best matched 20% sample and (d) 1S:3O structure best matched 33% sample. It is observed that the Zn-O bond distance increases with increasing S concentration. (e) The total DOS (tDOS) of the ZnO clusters with increasing lattice constants (representative of structural distortion induced by S incorporation) zoned in on the bandgap portion to illustrate the effect that the wurtzite ZnO lattice elongation has on bandgap.

The structures that were simulated, had much lower concentrations of S than suggested by XPS because the large DOS surrounding S atoms has a drastic effect[31] on the calculated XANES spectra. For this reason, the structural solutions are not entirely representative of our samples, but exhibit trends that are consistent with variations in S concentrations.

The focus will now shift from the electronic structure to the trends obtained from the geometric structural solutions and the relationship that exists between the two. We have already seen that incorporation of S leads to hybridization of its 3p orbitals to the conduction band, which changes the geometric structure. The change in structure results in a change of the relative ionicities of the atoms. This is further evidenced in the Zn_4O tetrahedrons for the different simulated structures shown in Fig. 4a-d, where the changes in the ionicity can be tracked by distortions in bond length of the Zn-O bonds. In general, as the S concentration increases, the Zn – O bonds get longer, supporting the fact that the ionicity of Zn increases[32] (Fig. 4a-d). This trend is also verified by Bader atomic charge

calculations, which showed that Zn accumulates more electrons, thereby reducing the total positive charge residing on each Zn atom (ESI Table S6).

From the simulated structural solutions, it is seen that one is capable of predicting the ionicity as discussed above which directly affects the bandgap, an important metric for a buffer layer. Also differences in Zn-O bond distance would surely change the catalytic activity of the film. To investigate the effect of bond lengthening on Zn-O, the lattice constants of wurtzite ZnO cluster were increased (from a pure wurtzite ZnO past a wurtzite ZnS) and the resulting clusters were simulated in FEFF. The total density of states (tDOS) was plotted, where we focused on the bandgap portion of the plot (Fig. 4e). As the distance increases in between the Zn and O atoms, the bandgap tends to get smaller and sharper resonances are formed in the near edge X-ray absorption fine structure (NEXAFS) region (Figures 4e and 1a). There are two opposing effects that cause the bowing effect of the bandgap that is observed in Zn(O,S) films (Fig. S7) and in literature.[5,12,17] On one hand, (1) the introduction of S, which acts as an electron donating ligand[33] causes an increase in the covalency of the Zn(O,S) films which tends to increase the bandgap and (2) the incorporation of S also stretches the Zn-O bonds increasing the ionicity of the crystal lattice, which acts to decrease the bandgap. At a certain point, the increase of S will no longer increase the Zn-O bond distance and so the increase in covalency will dominate, increasing the bandgap towards ZnS. This bowing phenomenon is the principal reason why Zn(O,S) has garnered so much attention, allowing one to tune the bandgap by nearly 1 eV (Fig. S7).

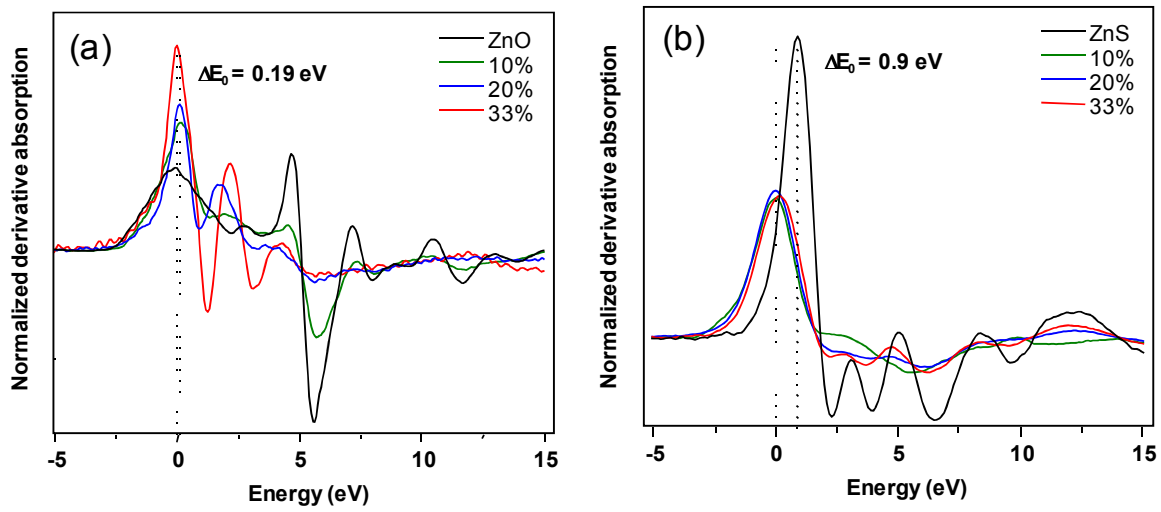

Fig. 5. (a) Normalized derivative of O K-edge XANES for ZnO and Zn(O,S) films with varied S content. With the presence of S, the E_0, which is defined as the absorption edge (conduction band onset) shifts to slightly higher energies. The ΔE_0 value listed is the difference between the ZnO and 20% sample. (b) Normalized derivative of S K-edge XANES for ZnS and Zn(O,S) films with varied S content. The ΔE_0 listed is the difference between the ZnS and 20% sample; the presence of O shifts the conduction band onset to lower energies.

From the derivative XANES spectra (Fig. 5) one can obtain how the conduction band onset is changing. At the O K-edge (Fig. 5a) the presence of S acts to shift the conduction band onset to slightly higher energies with respect to ZnO. The difference between ZnO and 20% sample is +0.19 eV. At the S K-edge (Fig. 5b), the presence of O brings the absorption edge to lower energies. The difference between ZnS and 20% sample is -0.9 eV. Varying the stoichiometry and monitoring the derivative of the XANES spectra at either edge can thus aid in tuning the conduction band offset. This acts as a direct rheostat for relative conduction band offsets.

In conclusion, we present a thorough investigation of the electronic and atomic structure of Zn(O,S) thin films deposited by ALD with chemical compositional tuning. The atomic specificity and ability to probe local character of the XAS technique allowed for a detailed exploration of local chemical and local structural modifications measured and analyzed for both ligands in the prepared films. We observe that despite having the same oxidation state and some degree of crystallinity, there are measurable differences in the XANES spectra

coming from the introduction of a second anion, indicating significant orbital mixing of the anion p-orbital to the conduction band. Quantum FEFF simulations of the XAS spectra and pDOS calculations on stoichiometries with lower S content capture all salient features of experimental data, and clearly show the mixed S 3p – Zn 4sp – O 2p character of the near-edge features. A qualitative description of the molecular orbital mixing for ZnS and Zn(O,S) is derived based on ligand-field theory, which provides insight into the nature of the lowest lying states in the NEXAFS spectra. The simulated structures gave insight into the ionicity of the atoms in the system, which helps in predicting relative bandgaps. We interestingly found that the inclusion of increasing concentrations of S initially acts to elongate the Zn-O bond distance, decreasing the bandgap, while at much higher S concentrations the increasing covalency dominates and bandgap again increases. Combining experimental and theoretical results, this work provides a route towards obtaining structural solutions and predicting properties of ALD deposited oxysulfide thin films in order to optimize its many tunable electrical, chemical and catalytic properties.

ESI

Electronic Supplementary Information (ESI) available: Details of the computational simulations and experimental measurements.

Acknowledgment

The authors would like to thank SNSF for use of PHI VersaProbe Scanning XPS Microprobe for XPS measurements and PANalytical X'Pert PRO x-ray diffraction system for GIXRD measurements. We also want to thank SLAC for allowing us to gather data using beamlines 4-3 and 10-1 at SSRL. We gratefully acknowledge partial support from Center on Nanostructuring for Efficient Energy Conversion (CNEEC) at Stanford University, an Energy Frontier Research Center funded by the U.S. Department of Energy, Office of Science, Office of Basic Energy Sciences under Award Number DE-SC0001060. We thank K. Roelofs and S. Bent for materials and consultations.

The Diversifying Academia Recruiting Excellence of Stanford University funded Dr. Orlando Trejo. Dr. Jan Torgersen was funded by the Austrian Research Fund (FWF) under the contract J3505-N20.

References

1 B. W. Sanders and A. Kitai, *Chem. Mater.*, 1992, **4**, 1005–1011.

2 S. K. Pandey, S. Pandey, A. C. Pandey and G. K. Mehrotra, *Appl. Phys. Lett.*, 2013, **102**, 233110.

3 P. Sinsermsuksakul, K. Hartman, S. Bok Kim, J. Heo, L. Sun, H. Hejin Park, R. Chakraborty, T. Buonassisi and R. G. Gordon, *Appl. Phys. Lett.*, 2013, **102**, -.

4 M. Buffière, S. Harel, C. Guillot-Deudon, L. Arzel, N. Barreau and J. Kessler, *Phys. status solidi*, 2015, **212**, 282–290.

5 S. K. Pandey, S. Pandey, V. Parashar, R. S. Yadav, G. K. Mehrotra and A. C. Pandey, *Nanoscale*, 2014, **6**, 1602–1606.

6 L. Sun, R. Haight, P. Sinsermsuksakul, S. Bok Kim, H. H. Park and R. G. Gordon, *Appl. Phys. Lett.*, 2013, **103**, -.

7 C. Platzer-Björkman, J. Lu, J. Kessler and L. Stolt, *Thin Solid Films*, 2003, **431-432**, 321–325.

8 N. Naghavi, S. Spiering, M. Powalla, B. Cavana and D. Lincot, *Prog. Photovoltaics Res. Appl.*, 2003, **11**, 437–443.

9 Q. Guo, G. M. Ford, W.-C. Yang, B. C. Walker, E. A. Stach, H. W. Hillhouse and R. Agrawal, *J. Am. Chem. Soc.*, 2010, **132**, 17384–6.

10 H. H. Park, A. Jayaraman, R. Heasley, C. Yang, L. Hartle, R. Mankad, R. Haight, D. B. Mitzi, O. Gunawan and R. G. Gordon, *Appl. Phys. Lett.*, 2014, **105**, -.

11 H. Hejin Park, R. Heasley and R. G. Gordon, *Appl. Phys. Lett.*, 2013, **102**.

12 C. Platzer-Bjorkman, T. Torndahl, D. Abou-Ras, J. Malmstrom, J. Kessler and L. Stolt, *J. Appl. Phys.*, 2006, **100**, 44506.

13 S. J. L. Billinge and I. Levin, *Science*, 2007, **316**, 561–5.

14 C. Bugot, N. Schneider, M. Jubault, D. Lincot and F. Donsanti, *J. Vac. Sci. Technol. A*, 2015, **33**, 01A151.

15 M. N. Mullings, C. Hägglund, J. T. Tanskanen, Y. Yee, S. Geyer and S. F. Bent, *Thin Solid Films*, 2014, **556**, 186–194.

16 J. R. Bakke, K. L. Pickrahn, T. P. Brennan and S. F. Bent, *Nanoscale*, 2011, **3**, 3482–508.

17 J. R. Bakke, J. T. Tanskanen, C. Hägglund, T. A. Pakkanen and S. F. Bent, *J. Vac. Sci. Technol. A*, 2012, **30**, 01A135.

18 U. Malm, J. Malmström, C. Platzer-Björkman and L. Stolt, *Thin Solid Films*, 2005, **480-481**, 208–212.

19 K. Ramanathan, J. Mann, S. Glynn, S. Christensen, J. Pankow, J. Li, J. Scharf, L. Mansfield, M. Contreras and R. Noufi, *Photovolt. Spec. Conf. (PVSC), 2012 38th IEEE*, 2012, 1677–1681.

20 J. J. Rehr, J. J. Kas, M. P. Prange, A. P. Sorini, Y. Takimoto and F. Vila, *Comptes Rendus Phys.*, 2009, **10**, 548–559.

21 J. J. Rehr, J. J. Kas, F. D. Vila, M. P. Prange and K. Jorissen, *Phys. Chem. Chem. Phys.*, 2010, **12**, 5503–5513.

22 S. Zhang, Y. Du, H. Li, W. Chu, J. Li, W. Yan, S. Wei, C. Yan and Z. Wu, *J. Phys. Chem. C*, 2009, **113**, 4263–4269.

23 B. Gilbert, B. H. Frazer, H. Zhang, F. Huang, J. F. Banfield, D. Haskel, J. C. Lang, G. Srajer and G. De Stasio, *Phys. Rev. B*, 2002, **66**, 245205.

24 D. Li, G. M. Bancroft, M. Kasrai, M. E. Fleet, X. H. Feng, K. H. Tan and B. X. Yang, *J. Phys. Chem. Solids*, 1994, **55**, 535–543.

25 R. J. Iwanowski, Z. Gol, A. Traverse, S. Pizzini, A. Fontaine, I. Winter and J. Hormes, *Phys. Rev. B*, 1996, **53**, 1119.

26 K. Nakanishi and T. Ohta, *J. Phys. Condens. Matter*, 2009, **21**, 104214.

27 D. Li, G. M. Bancroft, M. Kasrai, M. E. Fleet, B. X. Yang, X. H. Feng, K. Tan and M. Peng, *Phys. Chem. Miner.*, 1994, **20**, 489–499.

28 G. U. V. O. Æ. R. T. J. Æ. A. R. Gerson, 2005, **3**, 255–268.

29 B. V Gabrelian, A. A. Lavrentyev and I. Y. Nikiforov, *Phys. status solidi*, 1999, **215**, 1041–1047.

30 F. Jalilehvand, *Chem. Soc. Rev.*, 2006, **35**, 1256–1268.

31 O. Sipr, *J. Phys. Condens. Matter*, 2001, **13**, 4291.

32 K. J. Rao and J. Wong, *J. Chem. Phys.*, 1984, **81**, 4832–4843.

33 A. L. Dadlani, P. Schindler, M. Logar, S. P. Walch and F. (Fritz) B. Prinz, *J. Phys. Chem. C*, 2014.

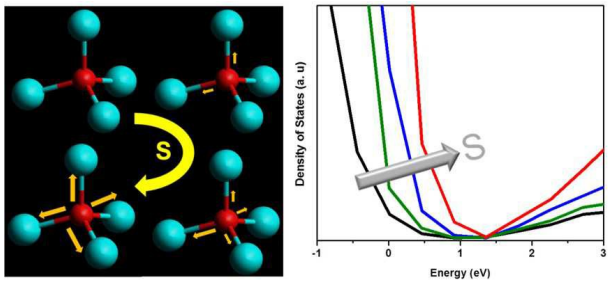

This work explains the bowing effect of the band gap as a result of the changing S concentration in Zn(O,S)